Bull. Chem. Soc. Ethiop. **2025**, 39(10), 2095- 2110.
DOI: https://dx.doi.org/10.4314/bcse.v39i10.15

ISSN 1011-3924
Printed in Ethiopia
Online ISSN 1726-801X

# ONE POT SYNTHESIS AND CHARACTERIZATION OF VISIBLE LIGHT RESPONSIVE ZnO/CuO COMPOSITES FOR EFFICIENT PHOTOCATALYTIC DEGRADATION OF METHYLENE BLUE

Mekya Yimam Ahmed[1‡], Biniyam Abdu Berehe[1‡], Daniel Manaye Kabtamu[2], Gangaraju Gedda[3], Ayalew H. Assen[1,4], Shewaye Lakew Mekuria[5], Myung-Geol Pang[3*], Wubshet Mekonnen Girma[1,3*]

[1]Department of Chemistry, College of Natural Science, Wollo University, P.O. Box:1145, Dessie, Ethiopia
[2]Department of Chemistry, Debre Berhan University, P. O. Box: 445, Debre Berhan, Ethiopia
[3]Department of Animal Science & Technology and BET Research Institute, Chung-Ang University, Anseong, Gyeonggi-do 17546, Republic of Korea
[4]Applied Chemistry and Engineering Research Centre of Excellence (ACER CoE), Mohammed VI Polytechnic University (UM6P), Lot 660 - Hay Moulay Rachid, 43150 Ben Guerir, Morocco
[5]Department of Chemistry, College of Natural and Computational Sciences, University of Gondar, 196, Gondar, Ethiopia

[‡]Mekya Yimam Ahmed and Biniyam Abdu Berehe contributed equally to this work.

(Received March 12, 2025; Revised June 16, 2025; Accepted June 25, 2025)

**ABSTRACT**. Industrial wastewater is a major contributor to water pollution, posing significant health risks and necessitating effective purification to prevent resource contamination. Organic dyes, widely used in textile, leather, paper, and pulp industries, as well as in academic research, can pollute water bodies if discharged untreated. This study utilized a biogenic approach to synthesize ZnO/CuO composite photocatalysts with varying CuO loadings (10%, 20%, 30%; denoted ZnO/CuO-10, ZnO/CuO-20, ZnO/CuO-30) using *Laggera tomentosa* plant extract, selected for its abundant phytochemicals, as a reducing and capping agent. These catalysts were characterized using scanning electron microscopy, X-ray diffraction, Fourier transform infrared spectroscopy, and diffuse reflectance spectroscopy. The photocatalytic performance was evaluated by degrading methylene blue (MB) under visible light. Results showed enhanced efficiency compared to pristine ZnO (65%), with ZnO/CuO-30 (70%), ZnO/CuO-20 (79%), and ZnO/CuO-10 (87%) degrading MB effectively. The superior performance of ZnO/CuO-10 is attributed to its optimized p-n heterojunction between ZnO (n-type) and CuO (p-type), which enhances charge separation and reduces electron-hole recombination, as evidenced by its high pseudo-first-order rate constant. The ZnO/CuO-10 catalyst also demonstrated stability over five reuse cycles. Overall, these biogenically synthesized composites, particularly ZnO/CuO-10, offer a viable and sustainable option for water remediation.

**KEY WORDS**: Photocatalysis, ZnO/CuO composite, Plant extract, Methylene blue degradation, Reusability

## INTRODUCTION

The rapid expansion of industries, particularly textiles and dyeing, has significantly polluted natural water resources through the discharge of untreated wastewater into rivers and lakes, compounded by atmospheric deposition [1]. Textile wastewater, laden with synthetic dyes, is a major contributor, releasing toxic, non-biodegradable, and carcinogenic pollutants that harm human health and aquatic ecosystems [2]. Among these, methylene blue (MB), a widely used cationic dye, is particularly concerning due to its toxicity, causing allergies, mutations, and respiratory distress, while disrupting aquatic photosynthesis by blocking light, leading to oxygen

*Corresponding authors. E-mail: mgpang@cau.ac.kr and wubshet.mekonnen@wu.edu.et

depletion [3]. Efficient and sustainable methods to remove MB from wastewater are urgently needed to safeguard human health and ecological integrity. While treatments like adsorption, biosorption, and membrane technology are used, they often suffer from low effectiveness, high costs, or secondary pollutant generation [4]. Photocatalysis, exploiting solar energy, offers a promising, eco-friendly alternative for degrading organic dyes with reusable catalysts [5].

Nanomaterials have recently been used as efficient materials for the removal of dyes through photocatalytic degradation owing to their different sizes, shapes, and forms [6]. These features arise from their distinct physicochemical properties including unique structures, exceptional mechanical durability, high surface-to-volume ratio, and superior thermal and electrical conductivities [7]. Therefore, various types of nanomaterials, including those containing titanium, silver, copper, gold, and zinc, have been used for the treatment of dye-polluted wastewater through decolourisation, precipitation, adsorption, and decomposition/degradation [8, 9]. Moreover, semiconducting metal oxides, such as ZnO [10], $Fe_2O_3$, $SiO_2$ [11], and $TiO_2$ [12], have been employed as photocatalysts. Among them, ZnO exhibits high photosensitivity and electron mobility, making it a remarkable photocatalytic material [13, 14]. Therefore, ZnO is also commonly used to degrade certain organic dyes such as MB. However, ZnO has a broad bandgap of 3.37 eV and high exciton binding energy of 60 meV. The high recombination rate of photogenerated electron–hole pairs, limited absorption of visible light, and high bandgap energy make ZnO unsuitable for photocatalytic treatments [15, 16]. To address these challenges, ZnO heterojunctions integrated with narrow-bandgap nanoparticles (NPs) have been developed to improve ZnO's visible light absorption and reduce charge recombination rates [17].

Different nanostructures can be used to create composites or hybrid materials with superior properties. Compared to other forms, composite nanomaterials have a larger surface area, resulting in more reactive sites, faster electron and mass transfers, and higher efficacy [18]. Consequently, the use of composite nanomaterials can not only considerably expand the scope of their applications but also successfully overcome the disadvantages of specific materials.
CuO NPs have gained considerable attention due to their distinct chemical and physical properties in relation to those of other NPs [19]. Copper is more widely used in optical, antibacterial, catalytic, and electrical applications owing to its easy accessibility, low cost, environmental friendliness, low toxicity, and suitable oxidation properties [20]. Consequently, materials with enhanced chemical reactivity, stability, photocatalytic activity, and sensing performance can be produced. ZnO/CuO composites have garnered significant interest for the photodegradation of organic pollutants due to their unique optical, electrical, and magnetic properties [21]. They are nontoxic to the environment and exhibit good catalytic properties.

Various methods, including photochemical, biochemical, physical, ultrasonication, and electrochemical processes, have been investigated for synthesizing metal NPs. However, these approaches often rely on toxic, expensive chemicals, incur high production costs, or result in incomplete purification. These challenges hinder industrial-scale production due to elevated costs, difficulties in large-area deposition, and strict environmental regulations. Green synthesis provides a solution through a simple, cost-effective, and environmentally friendly approach. By using water as a solvent, it reduces toxicity and streamlines the reaction process, making it ideal for metal NP production [17].Using natural resources like plant leaves for green synthesis provides an eco-friendly approach. Biological methods offer several advantages: (i) cost-effective and nontoxic; (ii) no need for stabilizing or capping agents, harmful chemicals, or organic solvents; (iii) no high-temperature conditions required; and (iv) suitable for large-scale production [22] . Momeni et al. recently described a method for synthesizing metal NPs using plant extracts or tree gums [21]. However, there is a lack of research focusing on the use of plant leaves as reducing agents in the synthesis of composites and evaluating their performance in dye degradation applications.

We synthesized ZnO/CuO composites using *Laggera tomentosa* as a reducing and capping agent via the co-precipitation method, with varying CuO content (10%, 20%, and 30%, denoted

as ZnO/CuO-10, ZnO/CuO-20, and ZnO/CuO-30, respectively). The composites, along with pure CuO and ZnO NPs, were characterized using XRD, SEM-EDS, FTIR, and DRS to assess crystallinity, morphology, functional groups, and optical properties. MB degradation performance under visible light showed efficiencies of 65% for ZnO, 70% for ZnO/CuO-30, 79% for ZnO/CuO-20, and 87% for ZnO/CuO-10 after 80 minutes, with ZnO/CuO-10 exhibiting the highest efficiency.

## EXPERIMENTAL

### *Chemicals and reagents*

Analytical-grade isopropanol (IPA; 99%), sodium hydroxide (NaOH; 99%), ethylenediaminetetraacetic acid (EDTA; 99%), copper sulfate pentahydrate ($CuSO_4 \cdot 5H_2O$; 99%), zinc sulfate hexahydrate ($ZnSO_4 \cdot 6H_2O$; 98%), Copper nitrate mono hydrate ($Cu(NO_3)_2 \cdot H_2O$, 99%) methylene blue (MB; 99%), and ethanol ($C_2H_5OH$; 99%) were employed in this study. The reagents and solvents were used without purification.

### *Plant material collection and extract preparation*

Fresh *Laggera tomentosa* plant material was collected from the desert area of Tossa Mountain in Southern Wollo, Ethiopia. The *Laggera tomentosa* leaves were washed multiple times with tap water and distilled water to remove dust and contaminants from the plant surface. The leaves were then air-dried at ambient temperature and crushed. The aqueous extract samples were produced by boiling 10 g of leaves in a flask containing 100 mL distilled water under magnetic stirring for 25 min at 80 °C. The resulting solution was cooled to ambient temperature and filtered through Whatman No. 1 filter paper. The filtrate was then transferred to a 150 mL conical flask for further use [23].

### *Laggera tomentosa plant extract assisted synthesis of CuO NPs*

CuO NPs were prepared by adding 15 mL of the aqueous plant extract solution to 20 mL of an aqueous 0.1M $CuSO_4 \cdot 5H_2O$ solution under continuous stirring until a uniform blue solution was obtained. The mixture was subsequently magnetically stirred at 80 °C for 2 h until a black precipitate was formed, which was then cooled to room temperature. The cooled precipitate was separated and rinsed twice using distilled water and ethanol to eliminate any remaining residues, followed by drying in an oven at 60 °C for 3 h. Finally, the resulting NPs were calcined at 400 °C for 4 h.

### *Laggera tomentosa plant extract assisted synthesis of ZnO NPs*

ZnO NPs were fabricated by dissolving 20 mL of 0.1M $ZnSO_4 \cdot 6H_2O$ in distilled water, followed by the addition of 15 mL. During stirring, a pale-yellow precipitate was formed, which was then boiled at 80 °C under magnetic stirring for 30 min to produce a white solution. The white solution was then centrifuged for 10 min, followed by washing with distilled water and ethanol. The product was collected and dried at 60 °C for 24 h, then calcined at 400 °C for 4 h.

### *Laggera tomentosa plant extract assisted synthesis of ZnO/CuO composites*

To synthesize ZnO/CuO composites (ZnO/CuO-10, ZnO/CuO-20, ZnO/CuO-30), 20 mL of 0.2M $ZnSO_4 \cdot 6H_2O$ was mixed with 30 mL of aqueous *Laggera tomentosa* leaf extract. The pH was adjusted to 10 by dropwise addition of a 1M NaOH solution, and the mixture was stirred at

80 °C for 30 min, resulting in a white suspension. The suspension was turned dark brown by dropwise addition of 20 mL $CuSO_4 \cdot 5H_2O$ solutions (0.02, 0.04, or 0.06M for 10%, 20%, or 30% CuO content, respectively). The solutions were heated and stirred at 90 °C for 2 h and then cooled to ambient temperature. The precipitates were separated by centrifugation at 5000 rpm for 20 min, dried at 60 °C for 24 h, and calcined at 400 °C for 2 h.

*Characterization*

A PerkinElmer FTIR spectrometer was used to identify the functional groups. Field emission SEM (FESEM; JSM 6500F, JEOL) was conducted to analyse the morphology of the composites. XRD was conducted to investigate the crystal phases, crystallinity, and particle sizes of the prepared NPs and composites; it was performed using a Shimadzu XRD-7000 instrument. MB was degraded using a tungsten lamp reactor (Japan, 150 W), and evaluated through DRS (Shimadzu-3600 Plus).

*Photocatalytic experiment*

MB degradation was carried out following a previously reported method [24]. The suspensions were first stirred in the dark for 30 min to reach adsorption/desorption equilibrium. Then, 25 mg of catalyst was added to 125 mL of 10 ppm MB solution (pH 7) in a 250 mL beaker. The mixture was irradiated under a 150 W tungsten lamp positioned 10 cm above the beaker, with continuous magnetic stirring and water cooling. A control experiment without catalyst was conducted to assess direct photolysis. At regular intervals, 5 mL aliquots were taken, centrifuged at 6000 rpm, and the supernatant's absorbance was measured at $\lambda$ = 663 nm using a UV-Vis spectrophotometer. Initial ($A_0$) and final ($A_t$) absorbance values were recorded. To evaluate reusability, 75 mg of the catalyst was mixed with 375 mL of 10 ppm MB solution and stirred for 30 min in the dark, followed by 80 min of visible light irradiation. After each cycle, the catalyst was recovered, washed with deionized water and acetone, dried, and reused in a fresh MB solution under the same conditions.

*Determination of active species*

To investigate the photocatalytic mechanism, scavenger experiments were conducted using $Cu(NO_3)_2$, IPA, and EDTA as scavengers for electrons, •OH radicals, and holes, respectively. In each test, 20 mL of 10 mM scavenger solution was added to 125 mL of 10 ppm MB solution containing 25 mg of ZnO/CuO-10 catalyst. The mixture was stirred under visible light irradiation for 80 minutes. Afterward, the absorbance was measured at the maximum wavelength of MB ($\lambda_{max}$ = 663 nm).

## RESULTS AND DISCUSSION

*Characterization of prepared NPs and composites*

Figure 1(a–f) shows the XRD patterns of the ZnO and CuO NPs and ZnO/CuO composites with different ratios. The XRD pattern of the ZnO NPs at the 2θ angles of 31.85°, 34.52°, 36.34°, 47.63°, 56.67°, 62.95°, 66.45°, 68.03°, 69.12°, 72.74°, and 77.03° corresponds to the (100), (002), (101), (102), (110), (103), (200), (112), (201), (004), and (202) planes, respectively (Figure 1(a)). These results are highly consistent with the development of hexagonal ZnO (JCPDS No.36-1451) containing zincite NPs [25]. The XRD pattern of the CuO NPs exhibits diffraction peaks at the 2θ angles of 32.58°, 35.64°, 38.87°, 48.88°, 53.62°, 58.36°, 61.66°, 66.24°, 68.10°, 72.55°, and 75.21°, which correspond to the (110), (002), (111), (20-2), (020),

(202), (11-3), (31-1), (113), (310) and (004) lattice indices, respectively (Figure 1(b)). The observed CuO NP peaks were ascribed to its monoclinic crystalline phase (JCPDS 048-1548) [26]. Figure 1(c–e) show the XRD patterns of the ZnO/CuO composites with different mass ratios. All composite catalysts showed both ZnO and CuO diffraction peaks.

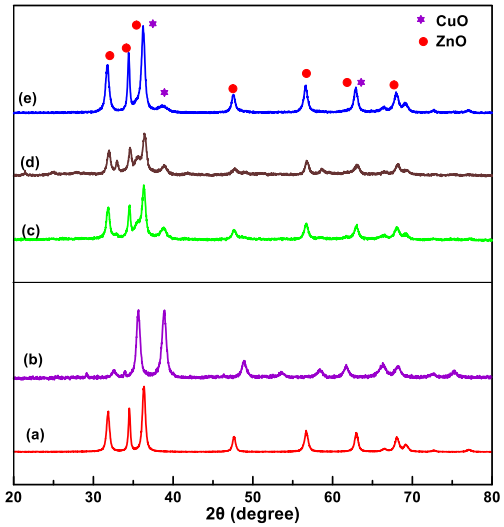


Figure 1. XRD patterns of (a) ZnO, (b) CuO, (c) ZnO/CuO-30, (d) ZnO/CuO-20 and (e) ZnO/CuO-10.

The XRD pattern of ZnO/CuO composites (Figure 1(e)) exhibits prominent ZnO peaks and less intense CuO peaks, attributed to reduced CuO concentration. CuO peaks appear at 2θ angles of 35.86°, 38.76°, and 61.66°, corresponding to the (002), (111), and (11-3) planes of the monoclinic structure, respectively, with the strongest peak at 38.76° (101) indicating dominance of the (101) facet. ZnO peaks are more intense than CuO peaks, confirming the predominance of ZnO in the composite structure [27].

The Debye–Scherrer equation was used to calculate the key structural parameters of each prepared NPs and composite, including the average crystallite size, dislocation density, and microstrain (equation (1)) [28].

$$D = \frac{K\lambda}{\beta Cos\theta} \quad (1)$$

$$\delta = \frac{1}{D2} \quad (2)$$

$$\varepsilon = \frac{\beta cos\theta}{4} \quad (3)$$

where K is Scherrer's constant (0.94), D is the size of the crystallite, λ is the X-ray wavelength, $\theta$ is the Bragg angle, and $\beta$ is the full-width half maximum, respectively. The dislocation density (δ) and microstrain (ε) in the samples were estimated using equations (2) and (3), respectively.

Crystallite size calculations showed a gradual decrease with increasing CuO content in the ZnO/CuO composites, consistent with the sizes of individual ZnO and CuO NPs. The crystallite sizes of all synthesized materials ranged from 10–25 nm (Table 1), with average microstrain decreasing as CuO content in the composites reduced [29].

Table 1. Average particle size, microstrain and dislocation density of CuO, ZnO, and ZnO/CuO with different ratio calculated using Scherrer's formula.

| NPs | Average crystalline size (nm) | Average microstrain ($\varepsilon$) | Average dislocation density ($\delta$) |
|---|---|---|---|
| CuO | 13.9 | 0.002637 | 0.005405 |
| ZnO | 21.0 | 0.001751 | 0.002375 |
| ZnO/CuO-30 | 15.6 | 0.002586 | 0.005899 |
| ZnO/CuO-20 | 16.1 | 0.002267 | 0.003954 |
| ZnO/CuO-10 | 18.3 | 0.002005 | 0.003106 |

The morphologies of the ZnO/CuO composites were examined using SEM (Figure 2). CuO displayed uneven, agglomerated particles with voids and pores (Figure 2 (a)), while SEM-EDS analysis confirmed the presence of Cu and O (Figure 2 (b)). ZnO displayed a morphology of irregularly distributed nanosheet-like particles without adhesion to voids or holes. SEM-EDS analysis confirmed the presence of only Zn and O, with no detectable impurities (Figure 2(c and d)). The ZnO/CuO composite morphology features agglomerated CuO particles dispersed over irregular nanosheet ZnO NPs. SEM analysis revealed moderate agglomeration with small, interconnected particles. EDS analysis of the composite showed an elemental composition of Zn (41.50%), Cu (8.16%), and O (50.35%) by atomic percentage, aligning with the ratios used in the synthesis process (Figure 2 (e and f)).

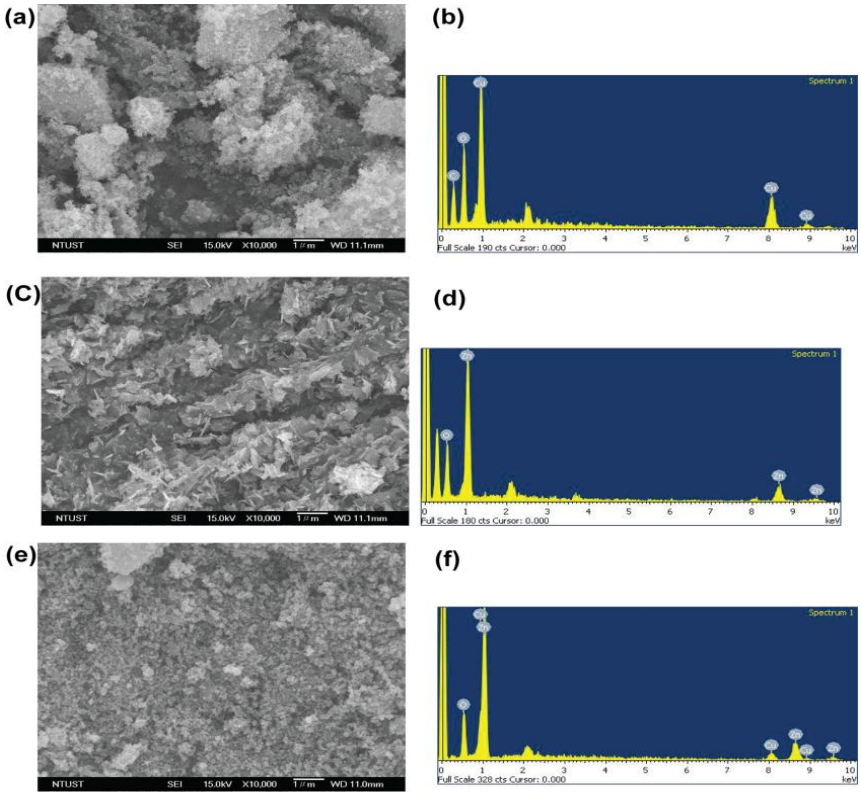


Figure 2. SEM images of (a) the CuO NPs, (c) ZnO NPs, and (e) ZnO/CuO-10. SEM-EDS results for (b) the CuO NPs, (d) ZnO NPs, and (f) ZnO/CuO-10.

FTIR analysis was conducted for characterisation and structural analysis of the composites. Figure 3 shows the FTIR spectra of the NPs and composites. The peaks at 1615 and 3450 $cm^{-1}$ were assigned to the C=O and OH searching vibrations, respectively (Figure 3(a)). The band at around 964 $cm^{-1}$ corresponds to the bending of carboxylic OH, confirming the existence of carboxyl groups in the *Laggera tomentosa* leaf extract. Flavonoids, tannins, proteins, polyphenols, alkaloids, saponins, terpenes, and vitamins are mainly comprised of carboxyl functional groups [30]. Plant-based chemicals facilitate the bio-reduction of metal salts into CuO and ZnO NPs and ZnO/CuO composites. FTIR spectra of these NPs and composites revealed distinct peaks, with those at 400–700 $cm^{-1}$ indicating the successful formation of Cu-O and Zn-O bonds in the CuO, ZnO NPs, and ZnO/CuO composites (Figure 3b–f) [31]. The major peaks observed in the plant extract were not observed in the composites because of the calcination process, which likely removed the plant extract from the composite surface.

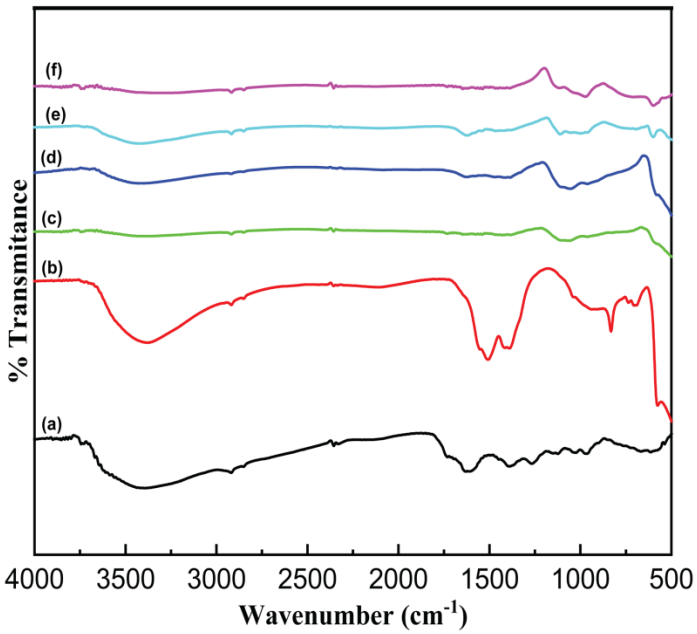


Figure 3. FTIR spectra of (a) the *Laggera tomentosa* plant extract, (b) CuO, (c) ZnO, (d) ZnO/CuO-30, (e) ZnO/CuO-20, and (f) ZnO/CuO-10.

*Optical properties and photocatalytic activities of the NPs and composites*

The optical properties of CuO, ZnO NPs, and ZnO/CuO composites were analyzed using DRS in the 320–800 nm wavelength range. The absorbance spectra of CuO, ZnO NPs, and ZnO/CuO composites (ZnO/CuO-30, ZnO/CuO-20, ZnO/CuO-10) showed broad absorption from 300–800 nm, with a prolonged tail at longer wavelengths (Figure 4(a)). ZnO NPs displayed broad absorption in the ultraviolet (UV) region due to their wide energy bandgap, while pure CuO absorbed in the visible region [21]. The composites (ZnO/CuO) exhibited enhanced absorbance edge and intensity, confirming the presence of CuO within the ZnO NPs. A precise estimate of the bandgap energy is critical for predicting the material properties. The Tauc relation was used to estimate the bandgaps of the CuO and ZnO NPs, as well as the ZnO/CuO composites [28].

The ZnO and CuO NPs and ZnO/CuO composites bandgap values were calculated by evaluating the optical data using Tauc's relation (equation (4)).

$$(\alpha h\nu)^{s} = A\ (h\nu - Eg) \quad (4)$$

where $\alpha$ is the optical absorption coefficient, $h\nu$ is the incident photon energy, s is a constant which represents the transition nature (s = 2 and ½ for direct and indirect bandgap energies, respectively), and $Eg$ is the optical bandgap energy.

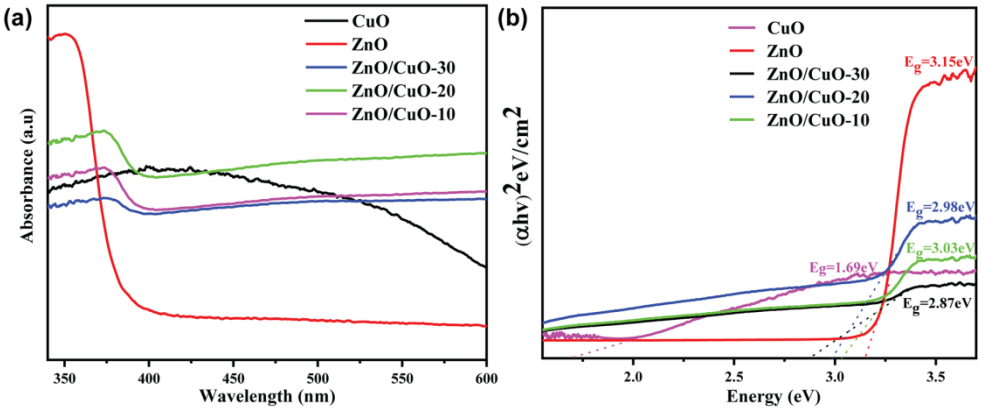


Figure 4. (a) DRS absorbance spectra and (b) $(\alpha h\nu)^2$ versus hν plot derived from the DRS absorbance spectra.

The bandgap energies of the CuO and ZnO NPs and ZnO/CuO-10, ZnO/CuO-20, and ZnO/CuO-30 were calculated to be 1.69, 3.15, 3.03, 2.98, and 2.87 eV, respectively (Figure 4(b)). The bandgap of the ZnO/CuO significantly reduced with an increasing CuO content in composites. The reduction in the bandgap enhances the ability of the ZnO/CuO composites to absorb visible light, reduces the occurrence of electron–hole recombination, and enhances their photocatalytic activity for MB degradation [24].

The photocatalytic performances of the prepared ZnO/CuO composites were evaluated for the selected target organic pollutant (MB). ZnO NPs alone and ZnO/CuO-30, ZnO/CuO-20, and ZnO/CuO-10 composites were incubated with MB under light to record their absorbance spectra. The percentage degradation efficiency was determined using equation (5):

$$\%D = \frac{A_0 - A_t}{A_o} \text{ X } 100\% \quad (5)$$

where $A_t$ represents the absorbance at time t (min) and $A_0$ represents the absorbance at t = 0 min.

The photocatalytic degradation efficiency of the ZnO-based nanocatalysts was assessed using visible light for 0–80 min using intervals of 20 min. The calculated MB degradation rates for the ZnO NPs, ZnO/CuO-30, ZnO/CuO-20, and ZnO/CuO-10 composites were 65, 70, 79, and 87%, respectively, as shown in Figure 5(a–d). ZnO/CuO-10 demonstrated the highest photocatalytic efficiency, achieving 87% MB degradation within 80 min, surpassing the other composites and pristine ZnO. This confirms the improved MB degradation efficiency of ZnO/CuO, which improves the transfer of electrons and decreases electron–hole recombination in the heterojunction system [32].

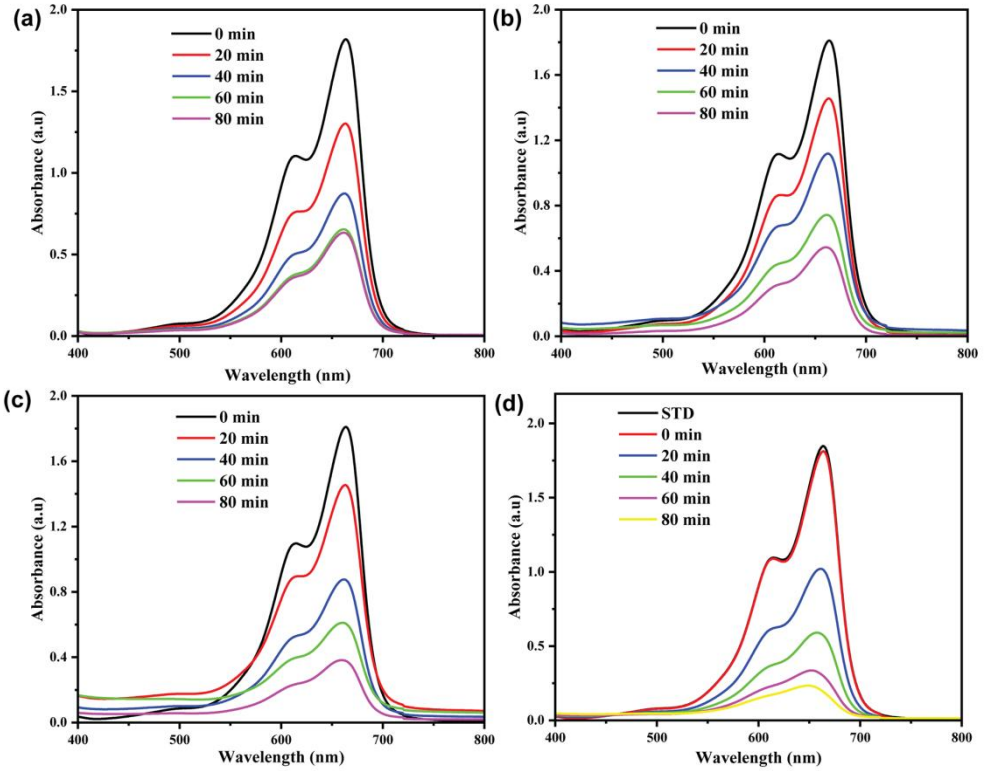


Figure 5. UV-visible absorption spectra for MB using (a) ZnO NPs (b) ZnO/CuO-30, (c) ZnO/CuO-20, and (d) ZnO/CuO-10 catalysts irradiated for different durations, STD mean MB standard.

*Kinetic study of MB dye degradation*

The pseudo-first-order photocatalytic reaction Langmuir-Hinshelwood kinetic model is the most well-known and frequently applied model for explaining the kinetics of photocatalysis in waste treatment. Pseudo-first-order degradation of MB by heterogeneous photocatalysts can be described using equation (6) [33].

$$\ln\left(\frac{At}{A0}\right) = -K_{app}\, t \qquad (6)$$

where t is the reaction time (min) and ($K_{app}$) represents the apparent pseudo-first-order rate constant ($min^{-1}$). $A_t$ and $A_0$ represent the UV absorption of the original MB in the linear function that plots $\ln(A_t/A_0)$ against time with a slope equal to ($K_{app}$).

Figure 6(a) shows the percentage degradation of MB, demonstrating that the degradation efficiency of each composite catalyst increased with contact time from 0 to 80 min. Among the composite catalysts, ZnO/CuO-10 exhibited the highest MB degradation. These findings demonstrate that MB degradation proceeds rapidly at first owing to the availability of empty sites, and then slows and ultimately reaches equilibrium, based on the catalyst dose, when the vacancies are filled and reduced.

The kinetics of the photocatalytic degradation of MB by the ZnO NPs and ZnO/CuO composites with different CuO content were estimated, and the results are shown in

Figure 6(b and c). Pseudo-first-order kinetics equation was used to determine the $K_{app}$ value for the MB degradation by the ZnO NPs and ZnO/CuO composites. Figure 6(c) shows the linear plots of $\ln(A_0/A_t)$ versus treatment time for the ZnO NPs, ZnO/CuO-30, ZnO/CuO-20, and ZnO/CuO-10. The $K_{app}$ values obtained from the slopes of the lines and the coefficient of linear regression were used to calculate the rate constant values, which were determined to be 0.014, 0.016, 0.020, and 0.0263 $min^{-1}$, respectively. The corresponding correlation coefficients ($R^2$) were 0.98076, 0.99524, 0.91438, and 0.9932. The dye degradation rate ultimately increased with time, as shown in Figure 6(b and c), where $A_0/A_t$ decreased over time and vice versa [34]. These results indicate that ZnO/CuO-10, as compared with the ZnO NPs, ZnO/CuO-30, and ZnO/CuO-20, exhibited higher photocatalytic activity for MB degradation. Among the composite catalysts, ZnO/CuO-10 exhibited the highest rate constant, which strongly agreed with the calculated $t_{1/2}$ (Figure 6(d)). The $t_{1/2}$ of each catalyst was calculated using equations (7) and (8).

$$\ln [A_t] = -K_t + \ln[A_0] \quad (7)$$

$$t_{1/2} = \frac{0.693}{K} \quad (8)$$

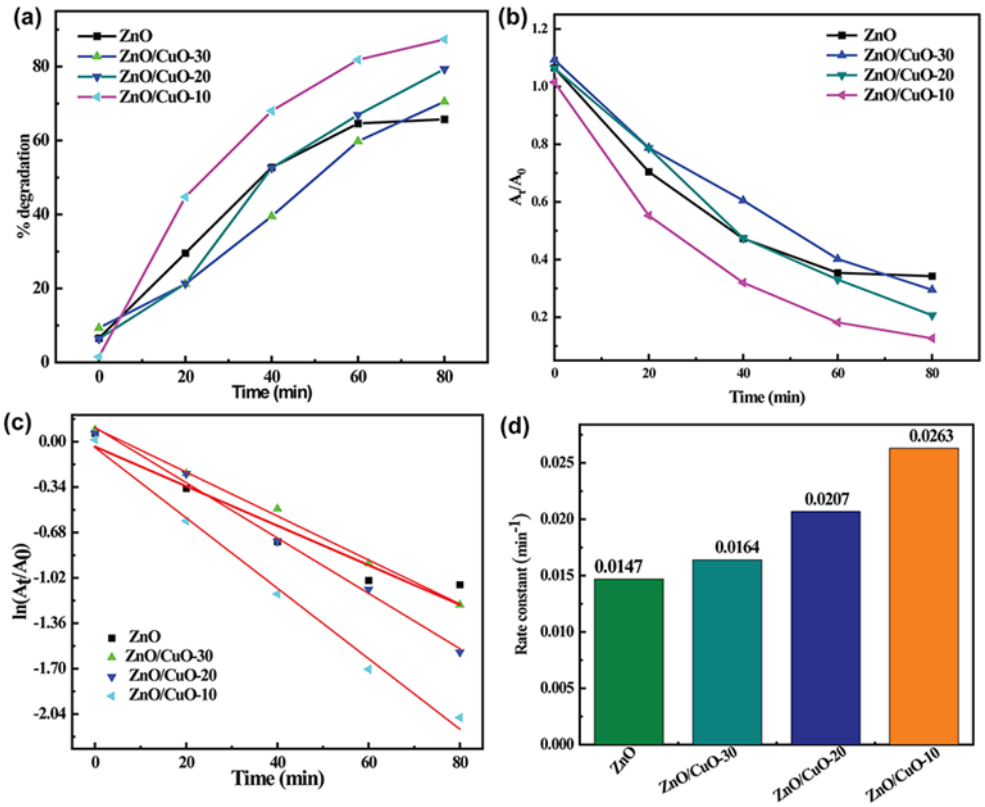


Figure 6. (a) Percentage degradation of MB using the different active catalysts. (b) Time degradation curve. (c) Pseudo-first-order kinetics linear fit data, rate constant ($K_{app}$), and ($R^2$). (d) Rate constant comparison of the various active catalysts in MB degradation.

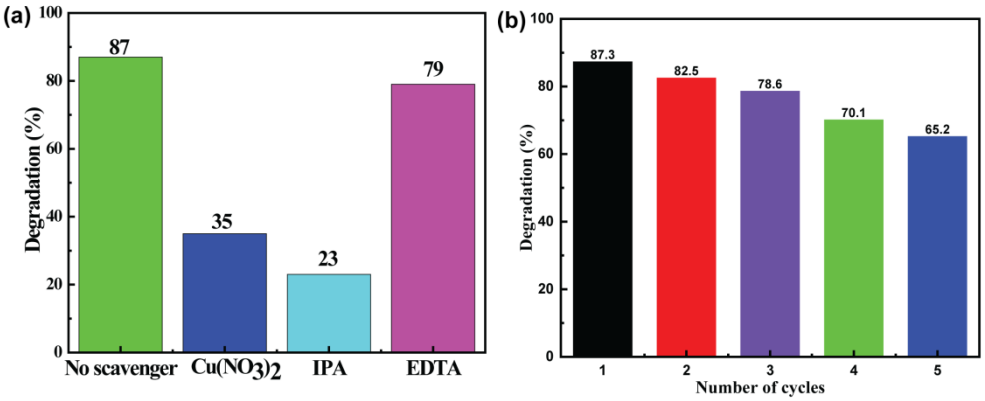


Figure 7. (a) Degradation of MB in various active species trapping solutions using 10% of ZnO/CuO catalyst. (b) Reusability of the ZnO/CuO-10 catalyst over five cycles.

To identify the surface-active species and elucidate the degradation mechanism, scavengers for charge carriers were used during MB degradation over the ZnO/CuO catalyst under visible light irradiation. The photocatalytic activity was evaluated by separately adding 0.1M EDTA, $Cu(NO_3)_2$, and IPA into the MB solution as scavengers for holes, electrons, and •OH radicals, respectively. As shown in Figure 7(a), the degradation efficiencies in the presence of EDTA, IPA, and $Cu(NO_3)_2$ were 79%, 23%, and 35%, respectively, compared to 87% without any scavenger. The lowest percentage degradation of MB occurred in the presence of IPA, ·OH radicals scavenger, confirming that ·OH radicals are the primary active species driving the photocatalytic degradation of MB with the most effective catalyst (ZnO/CuO-10).

The photodegradation rate was 87.3% during the initial cycle, and gradually decreased over the second, third, fourth, and fifth cycles to 82.5, 78.6, 70.1, and 65.2%, respectively (Figure 7(b)). After the fifth cycle, the degradation efficiency dropped by 22.1%, possibly due to the deactivation of some adsorption sites on the photocatalyst surface, leading to reduced photocatalytic activity, and/or a partial phase change in the dye solution under visible light exposure [24]. The ZnO/CuO-10 catalyst only exhibited a slight degradation decrease after three successive cycles, confirming that it is a promising reusable and effective catalyst. Moreover, the MB photodegradation efficiency using the ZnO/CuO composite under 80 min of light exposure was higher than that achieved with other nanomaterials, as compared to previously reported studies (Table 2).

In general, photocatalytic degradation efficiencies of the ZnO/CuO composites ZnO/CuO-10 (87%, 3.03 eV), ZnO/CuO-20 (79%, 2.98 eV), and ZnO/CuO-30 (70%, 2.87 eV) appear counterintuitive, as a smaller bandgap is expected to enhance visible light absorption and photocatalytic activity. However, the superior performance of ZnO/CuO-10 is attributed to its optimized p-n heterojunction between ZnO (n-type) and CuO (p-type), which enhances charge separation and reduces electron-hole recombination, as evidenced by its high pseudo-first-order rate constant (Kapp = 0.0263 $min^{-1}$, $R^2$ = 0.9932, Figure 6c). Additionally, SEM analysis (Figure 2e) reveals a well-dispersed morphology for ZnO/CuO-10, providing more active sites for methylene blue (MB) adsorption and degradation compared to the more agglomerated ZnO/CuO-20 and ZnO/CuO-30. The efficient generation of hydroxyl radicals (•OH) in ZnO/CuO-10 (Figure 7a) further contributes to its high efficiency. These factors heterojunction efficiency, surface morphology, and active species generation outweigh the bandgap advantage of ZnO/CuO-30, explaining the observed trend in MB degradation efficiencies.

Table 2. Comparison of the photocatalytic degradation performance of the 10% of ZnO/CuO composite with other reported catalysts.

| Type of catalyst | % of Degradation | Degradation time | Reference |
|---|---|---|---|
| CuO–ZnO (20%) | 82% | 105 min | [35] |
| 0.08CrZn | 85% | 90 min | [36] |
| CsLZnO-NPs | 80% | 240 min | [37] |
| ZnO-g-C3N4@PET | 92% | 120 min | [38] |
| *Parthenium hysterophorus*-Mediated ZnO | 55.69% | 32 min | [39] |
| $CeO_2$/ZnO | 88% | 210 min | [40] |
| 20% ZnO/Cu-DPA | 87% | 80min | [5] |
| Co-doped ZnO | 62.6% | 140 min | [41] |
| Ag-Zn | 85% | 60 min | [42] |
| $Fe_2O_3$/ZnO | 79% | 150 min | [43] |
| ZnO/CuO-10 | 87 % | 80 min | This work |

Figure 8 illustrates the photocatalytic degradation mechanism. The efficient separation of electron–hole pairs in the ZnO/CuO catalyst improves its catalytic activity and visible-light absorption [36]. CuO, a p-type semiconductor with a narrow bandgap of 1.35–1.79 eV [44], enhances the photocatalytic performance of ZnO NPs when added in optimal amounts. The valence band (EVB) and conduction band (ECB) energies were calculated using equations (9) and (10), respectively.

$$E_{VB} = x - E_e - 0.5E_g \quad (9)$$

$$E_{CB} = E_{VB} - E_g \quad (10)$$

where $x$ represents the absolute electronegativity of semiconductor (the reported $x$ values for CuO and ZnO are 5.81 and 5.79 eV, respectively) [45], $E_e$ represents the energy of free electrons in the hydrogen scale (approximately 4.5 eV), and the DRS-obtained bandgap energies for the ZnO and CuO NPs are 3.15 and 1.69 eV, respectively.

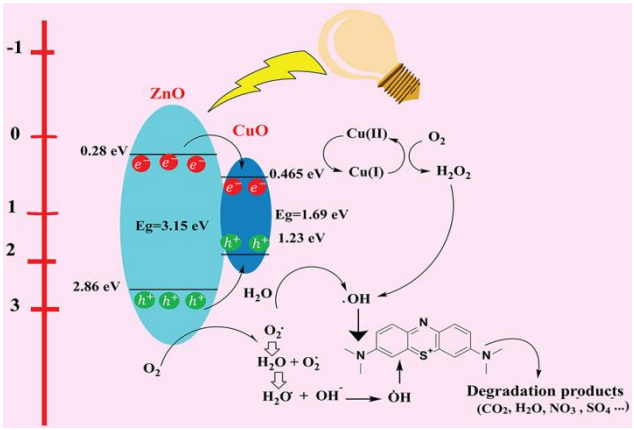


Figure 8. Photocatalytic degradation mechanism of MB degradation using the ZnO/CuO composite catalysts.

Effective separation of electron–hole pairs in the excited ZnO NPs enables efficient transfer of photo-induced electrons to CuO. The oxygen molecule is reduced to superoxide anion

radicals at the more negative potentials of ZnO's CB, driven by its lower redox potential (−0.33 eV for $O_2$ to $\bullet O_2^-$) [46]. However, the relatively high positive potential of the ZnO CB reduces its photocatalytic efficiency. Meanwhile, water oxidation to ·OH occurs at the more positive VB of ZnO. Radical generation is crucial for dye degradation. The photocatalytic reaction depends on MB adsorption onto the ZnO/CuO surface and efficient separation of photogenerated electron–hole pairs. Holes can react with surface-bound $OH^-$ to produce ·OH radicals. Adsorption equilibrium is disrupted, allowing MB molecules to transfer from the bulk solution to the catalyst surface, where they undergo redox reactions, ultimately degrading into $CO_2$, $H_2O$, and other intermediates. The CuO CB edge (0.465 eV) is insufficient to reduce $O_2$ to superoxide ($\bullet O_2^-$), but photoexcited electrons from ZnO can reduce Cu(II) to Cu(I). This Cu(I) then facilitates $O_2$ reduction to hydrogen peroxide ($H_2O_2$) via a Fenton/Fenton-like reaction. The generated $H_2O_2$ reacts with water and holes to produce additional ·OH radicals [47].

## CONCLUSIONS

Advances in nanotechnology have enabled the use of environmentally safe agents for effective removal of dye pollutants from wastewater. Visible light-responsive ZnO/CuO heterogeneous catalysts with varying CuO content were synthesized using a co-precipitation method. Zinc and copper salts were mixed with *Laggera tomentosa* plant extract, serving as both a reducing and capping agent, followed by annealing at 400 °C to produce the final composite catalysts. The synthesized ZnO/CuO composite catalysts were characterized using XRD, SEM-EDS, FTIR, and DRS. The optical properties of the composites revealed a decrease in the ZnO bandgap with increasing CuO content. Photodegradation efficiency studies demonstrated that the ZnO/CuO-10 catalyst achieved higher MB degradation (87%) compared to bare ZnO and other composite ratios. Active-species scavenging experiments identified electrons and OH radicals as the primary species responsible for MB degradation over the ZnO/CuO catalyst. The ZnO/CuO catalyst, synthesized by controlling CuO content, presents a promising alternative material for the photodegradation of organic pollutants in wastewater.

*Author contributions*

Mekya Yimam Ahmed: Methodology, Formal analysis, Investigation, Data curation, Validation, Biniyam Abdu Berehe: Methodology, Formal analysis, Investigation, Validation, Data curation, Writing - original draft. Daniel Manaye Kabtamu: Formal analysis, Validation, Data curation. Gangaraju Gedda: Formal analysis, Validation, Data curation. Ayalew H. Assen: Formal analysis, Validation, Data curation. Shewaye Lakew Mekuria: Formal analysis, Validation, Data curation. Myung-Geol Pang: Resources, Funding acquisition Wubshet Mekonnen Girma: Formal analysis, Software, Resources, Funding acquisition, Project administration, Supervision, writing- review editting.

*Conflicts of interest*

There are no conflicts to declare.

*Data availability*

The data that support the findings of this study are available from the corresponding author upon reasonable request.

## ACKNOWLEDGEMENTS

This study was supported by Wollo University through graduate student funding, Basic Science Research Program through the National Research Foundation of Korea (NRF), supported by the Ministry of Education (NRF-2018R1A6A1A03025159) and Brain Pool Program through the National Research Foundation of Korea (NRF), funded by the Ministry of Science and ICT (grant number: RS-2023-00236822). All the authors acknowledge Adama Science and Technology University for XRD and photocatalytic performance analysis and National Taiwan University of Science and Technology for SEM analysis.

## REFERENCES

1. Parvulescu, V.I.; Epron, F.; Garcia, H.; Granger, P. Recent progress and prospects in catalytic water treatment. *Chem. Rev.* **2022**, 122, 2981-3121.
2. Yang, G.; Zhang, D.; Zhu, G.; Zhou, T.; Song, M.; Qu, L.; Xiong, K.; Li, H. A Sm-MOF/GO nanocomposite membrane for efficient organic dye removal from wastewater. *RSC Adv.* **2020**, 10, 8540-8547.
3. Hacıosmanoğlu, G.G.; Genç, S.; Can, Z.S. Efficient removal of methyl orange from aqueous solutions using ulexite. *Environ. Technol. Innovation* **2021**, 22, 101466.
4. Ferenj, A.E.; Kabtamu, D.M.; Assen, A.H.; Gedda, G.; Muhabie, A.A.; Berrada, M.; Girma, W.M. Hagenia abyssinica-biomediated synthesis of a magnetic Fe3O4/NiO nanoadsorbent for adsorption of lead from wastewater. *ACS Omega* **2024**, 9, 6803-6814.
5. Berehe, B.A.; Assen, A.H.; Kumar, A.S.K.; Ulla, H.; Duma, A.D.; Chang, J.-Y.; Gedda, G.; Girma, W.M. Highly efficient visible light active ZnO/Cu-DPA composite photocatalysts for the treatment of wastewater contaminated with organic dye. *Sci. Rep.* **2023**, 13, 16454.
6. Sharma, S.; Kumar, K.; Thakur, N.; Chauhan, S.; Chauhan, M. The effect of shape and size of ZnO nanoparticles on their antimicrobial and photocatalytic activities: a green approach. *Bull. Mater. Sci.* **2020**, 43, 1-10.
7. Salem, S.S.; Fouda, A. Green synthesis of metallic nanoparticles and their prospective biotechnological applications: an overview. *Biol. Trace Elem. Res.* **2021**, 199, 344-370.
8. Ferenji, A.E.; Hassen, Y.E.; Mekuria, S.L.; Girma, W.M. Biogenic mediated green synthesis of NiO nanoparticles for adsorptive removal of lead from aqueous solution. *Heliyon* **2024**, 10, e31669.
9. Yimer, M.; Ansari, S.N.; Berehe, B.A.; Gudimella, K.K.; Gedda, G.; Girma, W.M.; Hasan, N.; Tasneem, S. Adsorptive removal of heavy metals from wastewater using Cobalt-diphenylamine (Co-DPA) complex. *BMC Chem.* **2024**, 18, 23.
10. Weldekirstos, H.D.; Zerie, M.; Manaye, D.; Tedla, A.; Negash, A. Effect of surfactants (cetyl trimethyl ammonium-bromide, ethyl di-tetra amine and polyacrylamide) on the synthesis of zinc oxide for photocatalytic application. *Bull. Chem. Soc. Ethiop.* **2024**, 38, 923-935.
11. Aguado, J.; Van Grieken, R.; López-Muñoz, M.-J.; Marugán, J. A comprehensive study of the synthesis, characterization and activity of TiO2 and mixed TiO2/SiO2 photocatalysts. *Appl. Catal. A* **2006**, 312, 202-212.
12. Lum, P.; Foo, K.; Zakaria, N.; Palaniandy, P. Ash based nanocomposites for photocatalytic degradation of textile dye pollutants: A review. *Mater. Chem. Phys.* **2020**, 241, 122405.
13. Bechambi, O.; Chalbi, M.; Najjar, W.; Sayadi, S. Photocatalytic activity of ZnO doped with Ag on the degradation of endocrine disrupting under UV irradiation and the investigation of its antibacterial activity. *Appl. Surf. Sci.* **2015**, 347, 414-420.
14. Olani, A.; Guyasa, J.N.; Nemera, D.J.; Efa, M.T.; Beyene, T.T. Impact of graphene oxide integration with ZnO nanoparticles on its photocatalytic, antimicrobial, and antioxidant activities. *Bull. Chem. Soc. Ethiop.* **2025**, 39, 515-534.

15. Amenu, B.; Taddesse, A.M.; Kebede, T.; Mengesha, E.T.; Bezu, Z. Polyaniline-supported MWCNTs/ZnO/$Ag_2CO_3$ composite with enhanced photocatalytic and antimicrobial applications. *Environ. Nanotechnol. Monit. Manage.* **2024**, 21, 100926.
16. Bezu, Z.; Taddesse, A.M.; Diaz, I. Natural zeolite supported g-C3N4/ZnO/Ag3PO4 composite: A tandem n-n heterojunction for simultaneous photodegradation of dyes under visible and solar irradiation. *J. Photochem. Photobiol. A* **2024**, 449, 115369.
17. Alsulmi, A.; Mohammed, N.N.; Soltan, A.; Messih, M.F.A.; Ahmed, M.A. Engineering S-scheme CuO/ZnO heterojunctions sonochemically for eradicating RhB dye from wastewater under solar radiation. *RSC Adv.* **2023**, 13, 13269-13281.
18. Das, S.; Srivastava, V.C. An overview of the synthesis of CuO-ZnO nanocomposite for environmental and other applications. *Nanotechnol. Rev.* **2018**, 7, 267-282.
19. Rathnakumar, S.S.; Noluthando, K.; Kulandaiswamy, A.J.; Rayappan, J.B.B.; Kasinathan, K.; Kennedy, J.; Maaza, M. Stalling behaviour of chloride ions: a non-enzymatic electrochemical detection of α-Endosulfan using CuO interface. *Sens. Actuators B* **2019**, 293, 100-106.
20. Grass, G.; Rensing, C.; Solioz, M. Metallic copper as an antimicrobial surface. *Appl. Environ. Microbiol.* 2011, 77, 1541-1547.
21. Momeni, S.S.; Nasrollahzadeh, M.; Rustaiyan, A. Green synthesis of the Cu/ZnO nanoparticles mediated by Euphorbia prolifera leaf extract and investigation of their catalytic activity. *J. Colloid Interface Sci.* **2016**, 472, 173-179.
22. Alamier, W.M.; Hasan, N.; Syed, I.S.; Bakry, A.M.; Ismail, K.S.; Gedda, G.; Girma, W.M. Silver nanoparticles' biogenic synthesis using *Caralluma subulata* aqueous extract and application for dye degradation and antimicrobials activities. *Catalysts* **2023**, 13, 1290.
23. Paramasivam, D.; Balasubramanian, B.; Suresh, R.; Kumaravelu, J.; Vellingiri, M.M.; Liu, W.-C.; Meyyazhagan, A.; Alanazi, A.M.; Rengasamy, K.R.R.; Arumugam, V.A. One-pot synthesis of silver nanoparticles derived from aqueous leaf extract of *Ageratum conyzoides* and their biological efficacy. *Antibiotics* **2023**, 12, 688.
24. Berehe, B.A.; Assen, A.H.; Kumar, A.S.K.; Ulla, H.; Duma, A.D.; Chang, J.Y.; Gedda, G.; Girma, W.M. Highly efficient visible light active ZnO/Cu-DPA composite photocatalysts for the treatment of wastewater contaminated with organic dye. *Sci. Rep.* **2023**, 13, 16454.
25. Jamil, S.; Tariq, T.; Khan, S.R.; Ehsan, M.A.; Rehman, A.; Janjua, M.R.S.A. Structural characterization, synthesis and application of Zincite nanoparticles as fuel additive. *J. Cluster Sci.* **2022**, 33, 1165-1176.
26. Veisi, H.; Karmakar, B.; Tamoradi, T.; Hemmati, S.; Hekmati, M.; Hamelian, M. Biosynthesis of CuO nanoparticles using aqueous extract of herbal tea (*Stachys Lavandulifolia*) flowers and evaluation of its catalytic activity. *Sci. Rep.* **2021**, 11, 1-13.
27. Cao, Y.; Dhahad, H.A.; El-Shorbagy, M.; Alijani, H.Q.; Zakeri, M.; Heydari, A.; Bahonar, E.; Slouf, M.; Khatami, M.; Naderifar, M. Green synthesis of bimetallic ZnO–CuO nanoparticles and their cytotoxicity properties. *Sci. Rep.* **2021**, 11, 1-8.
28. Muthuvel, A.; Jothibas, M.; Manoharan, C. Effect of chemically synthesis compared to biosynthesized ZnO-NPs using Solanum nigrum leaf extract and their photocatalytic, antibacterial and in-vitro antioxidant activity. *J. Environ. Chem. Eng.* **2020**, 8, 103705.
29. Kumari, V.; Yadav, S.; Jindal, J.; Sharma, S.; Kumari, K.; Kumar, N. Synthesis and characterization of heterogeneous ZnO/CuO hierarchical nanostructures for photocatalytic degradation of organic pollutant. *Adv. Powder Technol.* **2020**, 31, 2658-2668.
30. Hassan, S.E.-D.; Salem, S.S.; Fouda, A.; Awad, M.A.; El-Gamal, M.S.; Abdo, A.M. New approach for antimicrobial activity and bio-control of various pathogens by biosynthesized copper nanoparticles using endophytic actinomycetes. *J. Radiat. Res. Appl. Sci.* **2018**, 11, 262-270.
31. Jayaprakash, J.; Srinivasan, N.; Chandrasekaran, P.; Girija, E.K. Synthesis and characterization of cluster of grapes like pure and Zinc-doped CuO nanoparticles by sol-gel method. *Spectrochim. Acta Part A* **2015**, *136 Pt C*, 1803-1806.

32. Huang, H.; Li, F.; Wang, H.; Zheng, X. The size controlled synthesis of Cu 2 S/P25 hetero junction solar-energy-materials and their applications in photocatalytic degradation of dyes. *RSC Adv.* **2017**, 7, 50056-50063.
33. Muthuvel, A.; Jothibas, M.; Manoharan, C.; Jayakumar, S.J. Synthesis of $CeO_2$-NPs by chemical and biological methods and their photocatalytic, antibacterial and in vitro antioxidant activity. *Res. Chem. Intermed.* **2020**, 46, 2705-2729.
34. González, R.L.; de la Fuente, O.; García, R.L.; del Carmen Uribe López, M.; Owen, P.Q.; López, M.C.H.; Lemus, M.A.A. Effect of phenol concentration on the photocatalytic performance of ZnO nanoparticles. *J. Chem. Technol. Biotechnol.* **2023**, 98, 1826-1836.
35. Bekru, A.G.; Tufa, L.T.; Zelekew, O.A.; Goddati, M.; Lee, J.; Sabir, F.K. Green synthesis of a CuO–ZnO nanocomposite for efficient photodegradation of methylene blue and reduction of 4-nitrophenol. *ACS omega* **2022**, 7, 30908-30919.
36. Zelekew, O.A.; Fufa, P.A.; Sabir, F.K.; Duma, A.D. Water hyacinth plant extract mediated green synthesis of Cr(2)O(3)/ZnO composite photocatalyst for the degradation of organic dye. *Heliyon* **2021**, 7, e07652.
37. Şendal, K.; Üstün Özgür, M.; Gülen, J. Biosynthesis of ZnO photocatalyst and its application in photo catalytic degradation of methylene blue dyestuff. *J. Dispersion Sci. Technol.* **2023**, 44, 2734-2747.
38. Liu, X.Y.; Li, J. S-scheme heterojunction ZnO/g-C3N4 shielding polyester fiber composites for the degradation of MB. *Semicond. Sci. Technol.* **2021**, 36, 045025.
39. Nzilu, D.; Madivoli, E.; Makhanu, D.; Wanakai, S.; Kirui, G.; Mwangi, V.; Kareru, P. Synthesis and characterization of parthenium hysterophorus-mediated ZnO nanoparticles for methylene blue dye degradation. *J. Chem.* **2024**, 2024, 1088430.
40. Syed, A.; Yadav, L.S.R.; Bahkali, A.H.; Elgorban, A.M.; Abdul Hakeem, D.; Ganganagappa, N. Effect of CeO2-ZnO nanocomposite for photocatalytic and antibacterial activities. *Crystals* **2020**, 10, 817.
41. Vallejo, W.; Cantillo, A.; Salazar, B.; Diaz-Uribe, C.; Ramos, W.; Romero, E.; Hurtado, M. Comparative study of ZnO thin films doped with transition metals (Cu and Co) for methylene blue photodegradation under visible irradiation. *Catalysts* **2020**, 10, 528.
42. Idris, D.S.; Roy, A.; Subramanian, A.; Alghamdi, S.; Chidamabaram, K.; Qusty, N.F. Bio-fabrication of silver–zinc bimetallic nanoparticles and its antibacterial and dye degradation activity. *J. Inorg. Organomet. Polym. Mater.* **2024**, 34, 1908-1919.
43. Ameen, F.; Altuner, E.E.; Tiri, R.N.E.; Gulbagca, F.; Aygun, A.; Sen, F.; Majrashi, N.; Orfali, R.; Dragoi, E.N. Highly active iron(II) oxide-zinc oxide nanocomposite synthesized Thymus vulgaris plant as bioreduction catalyst: Characterization, hydrogen evolution and photocatalytic degradation. *Int. J. Hydrogen Energy* **2023**, 48, 21139-21151.
44. Chen, H.; Leng, W.; Xu, Y. Enhanced visible-light photoactivity of CuWO4 through a surface-deposited CuO. *J. Phys. Chem. C* **2014**, 118, 9982-9989.
45. Xu, Y.; Schoonen, M.A. The absolute energy positions of conduction and valence bands of selected semiconducting minerals. *Am. Mineral.* **2000**, 85, 543-556.
46. Naseri, A.; Samadi, M.; Mahmoodi, N.M.; Pourjavadi, A.; Mehdipour, H.; Moshfegh, A.Z. Tuning composition of electrospun ZnO/CuO nanofibers: Toward controllable and efficient solar photocatalytic degradation of organic pollutants. *J. Phys. Chem. C* **2017**, 121, 3327-3338.
47. Liu, Z.; Bai, H.; Xu, S.; Sun, D.D. Hierarchical CuO/ZnO "corn-like" architecture for photocatalytic hydrogen generation. *Int. J. Hydrogen Energy* **2011**, 36, 13473-13480.